Cryogenic Mechanical Alloying of Poly(methyl methacrylate) with Polyisoprene and Poly(ethylene-*alt*-propylene)

Archie P. Smith,[†,‡] Harald Ade,[*,§] C. Maurice Balik,[‡] Carl C. Koch,[‡] Steven D. Smith,[||] and Richard J. Spontak[*,‡,⊥]

Departments of Materials Science & Engineering, Physics, and Chemical Engineering, North Carolina State University, Raleigh, North Carolina 27695; and Corporate Research Division, The Procter and Gamble Company, Cincinnati, Ohio 45239

Received August 26, 1999

ABSTRACT: Mechanical alloying is performed at cryogenic temperatures to incorporate polyisoprene (PI) or its hydrogenated analogue poly(ethylene-*alt*-propylene) (PEP) into poly(methyl methacrylate) (PMMA) as an example of high-energy solid-state blending. Morphological characterization of the blends by X-ray and electron microscopies confirms that the degree of dispersion of the constituent polymers improves with increasing milling time. Such dispersion in the PEP/PMMA blends is, however, ultimately compromised by phase coarsening when the materials are postprocessed above the PMMA glass transition temperature in the melt. Milling-induced PI cross-linking serves to suppress phase coarsening in PI/PMMA blends, which remain relatively well-dispersed even after postprocessing. These blends are generally less fracture-resistant than the as-received PMMA due mainly to the accompanying reduction in PMMA molecular weight. Their optical transparency is observed to decrease dramatically with increasing PEP or PI concentration until they appear opaque. An overall improvement in blend properties by mechanical alloying is, however, anticipated upon judicious selection of more degradation-resistant polymers.

Introduction

An important technological route for overcoming the physical property limitations of homopolymers is to blend two or more homopolymers together in such fashion that yields specific multifunctional properties.[1,2] Blending techniques, however, typically rely on processing polymers as solutions or melts, wherein high chain mobility facilitates phase separation between intrinsically incompatible polymers. Although numerous strategies have been developed to improve polymer compatibility and lessen the degree of phase separation, they often involve additional time, expense, material, and process considerations, as well as environmental concerns.[3,4] An intriguing alternative to conventional polymer blending methodologies is high-energy solid-state blending. In this case, polymer chain mobility is drastically reduced, and the possibility of phase separation during blending is virtually eliminated. High-energy solid-state blending generally relies on mechanical agitation to mix two or more polymers. The possibility that such agitation may promote mechanical degradation of the constituent polymers has severely limited the commercial viability of solid-state blending. This shortcoming is, however, being surmounted in such emerging polymer processes as solid-state extrusion[5−7] and mechanical milling/alloying.[8−13]

Mechanical alloying refers to the high-energy ball milling of two or more dissimilar materials to produce powders in which the materials are intimately mixed on the molecular or atomic scale.[14] This technique, illustrated in Figure 1, produces nonequilibrium systems and novel materials, such as the oxide-dispersion-strengthened alloys initially developed for the aerospace industry.[15,16] With the subsequent discovery that mechanical alloying could yield amorphous metal alloys,[17] applications that employ mechanical alloying as a means of mixing inorganic materials have greatly increased and diversified.[14,18,19] The utility of mechanical alloying in obtaining unique multifunctional materials from commodity feedstock has not, however, extended to the organic materials arena until quite recently. Efforts designed to mechanically alloy organic materials now include both small organic molecules[20−23] and polymers.[8−13,24−26] While small improvements in the physical properties of polymer blends produced by mechanical alloying[8,11] have been reported, the morphological characteristics of such blends presently remain largely undetermined.

An important consideration in the general development of blend morphology and, consequently, blend properties is the nature and degree to which the constituent macromolecules change during processing. Two potential routes for alloying-induced blend modification are schematically depicted in Figure 1. Figure 1a shows that the mechanical action of high-energy ball milling may serve to co-pulverize polymer powder particles, thereby promoting a substantial physical reduction in the scale of dispersion within the system. While this result is nontrivial, the possibility of producing chemically coupled chains in situ (see Figure 1b) could constitute a more important result. The combination of shear, extension, fracture, and cold-welding experienced by polymer powder particles during mechanical alloying is expected to induce chain scission or hydrogen abstraction and, as a result, molecular

* To whom correspondence should be addressed.
[†] Present address: Polymers Division, National Institute of Standards & Technology, Building 224, Gaithersburg, MD 20899.
[‡] Department of Materials Science & Engineering, North Carolina State University.
[§] Department of Physics, North Carolina State University.
[||] The Procter and Gamble Company.
[⊥] Department of Chemical Engineering, North Carolina State University.

10.1021/ma991453v CCC: $19.00
Published on Web 03/17/2000

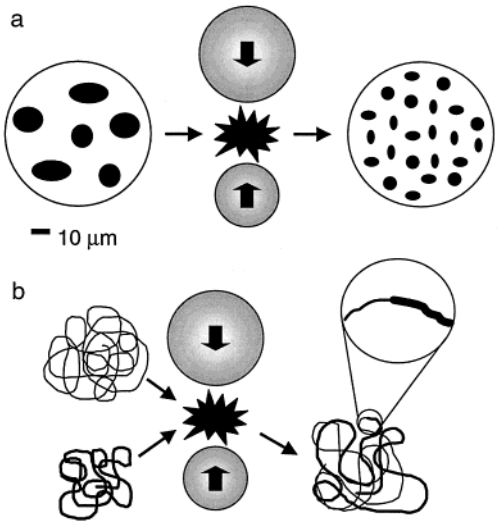

Figure 1. Schematic illustration showing the possible effects of solid-state mechanical alloying on polymer blends. In part a, high-energy impact between ball bearings promotes a physical reduction in the size scale of the blended polymers. Another effect is shown in part b, in which free radicals generated by chain scission chemically couple polymer chains and produce a more stable blend.

weight reduction and free radical formation. Reaction of free radicals from broken chains of the same polymer species could affect polymer miscibility and coalescence kinetics, whereas reaction of radicals from different chain species could produce block or graft copolymers as compatibilizing agents under the right set of conditions.

To discern the efficacy of cryogenic mechanical alloying in generating novel multiphase polymer systems, we have undertaken a study aimed at incorporating small quantities of polyisoprene (PI) or its hydrogenated analogue poly(ethylene-*alt*-propylene) (PEP) into the thermoplastic poly(methyl methacrylate) (PMMA). The rigorous requirements established[27−30] for a rubber dispersion to yield effective toughening ensure that the present study provides a useful test of the ability of mechanical alloying to produce polymer blends of commercial relevance. Toughening of PMMA is currently performed through the melt addition of multilayer core−shell particles, which are synthesized in a separate emulsion polymerization step.[31−33] Since PMMA is produced in high volume due to its excellent optical properties, a simpler method of rubber toughening offers great potential for economic impact. While the chemical similarity between PI and PEP makes these materials attractive candidates for comparison, it must be remembered that PEP is more resistant to radiation-induced degradation and possesses different chain statistics than PI (which could undergo chemical cross-linking at sites of unsaturation). A description of the effects of high-energy mechanical milling on each of the homopolymers employed here is provided elsewhere.[34] The present study details the ability of cryogenic mechanical alloying to produce highly dispersed polymer blends (PEP/PMMA and PI/PMMA) without ex situ compatibilization. Resultant blends are characterized here with respect to phase morphology, impact strength and optical clarity.

Experimental Section

Poly(methyl methacrylate) ($\bar{M}_n$ = 252 000, $\bar{M}_w/\bar{M}_n$ = 4.11) was purchased from Aldrich and used as-received, whereas the PI ($\bar{M}_n$ = 72 100, $\bar{M}_w/\bar{M}_n$ = 1.05) was synthesized via living anionic polymerization. A fraction of the PI was subsequently hydrogenated to form PEP. Molecular weight characteristics were determined from gel permeation chromatography. Binary PEP/PMMA and PI/PMMA mixtures were prepared by mechanical alloying performed at cryogenic temperatures so that all components were in the solid (glassy) state. Three grams of polymers in a predesignated mass ratio was placed in a hardened steel vial with 30 g of steel ball bearings (measuring 6.4 and 7.9 mm in diameter). The vial was then sealed under Ar (<10 ppm of O_2) and placed in a custom-designed nylon sleeve that allowed peripheral circulation of liquid nitrogen. A thermocouple monitored the external vial temperature during milling and ensured that the vial was maintained at −180 °C or below. The vial assembly was placed in a heavily reinforced SPEX 8000 mixer/mill and agitated for milling times (t_m) up to 10 h to produce a fine powder. After milling, the vial was allowed to return to ambient temperature and the powder was removed.

To analyze the morphology and stability of the resultant blends, several different samples were prepared by consolidating blend powders in a Carver press. In the first series, powders were pressed at ambient temperature (20 °C) and high pressure (700 MPa) for 15 min to retain the "as-milled" morphology of the blends. Morphological characteristics of blends under melt (extrusion) conditions were examined in samples pressed at 125 and 200 °C with lower pressure (17 and <1 MPa, respectively). These temperatures were maintained for 5 min before the samples were quenched to ambient temperature in a water bath. The resultant films were microtomed at −100 °C in a Reichert-Jung Ultracut S cryoultramicrotome to produce thin sections for scanning transmission X-ray microscopy (STXM) and transmission electron microscopy (TEM). Electron images of PI-containing blends, selectively stained with the vapor of 4% OsO_4(aq) for 90 min, were acquired on a Zeiss EM902 electron spectroscopic microscope at an accelerating voltage of 80 kV and at energy loss settings of 40−120 eV.

In addition, STXM was performed on the microscope located at the National Synchrotron Light Source at Brookhaven National Laboratory. This instrument utilized a high-intensity, tunable soft X-ray source in conjunction with a diffraction monochromator to provide a coherent X-ray source with an energy resolution of about 150 meV at the C K-edge.[35] The X-ray source was focused by a diffractive optical element (zone plate) into a microprobe with a full width at half-maximum of about 45 nm.[36] A section was placed in the microprobe, and the transmitted flux was recorded in one of two operating modes. In the first mode, the photon energy was held constant and the sample was raster-scanned to yield a position-dependent absorbance map, whereas the second maintained constant sample position so that the photon energy could be varied to produce a near-edge X-ray absorption fine structure (NEXAFS) spectrum.[37] Since X-ray absorption occurs when an inner shell electron is promoted into an unoccupied molecular orbital by an incident photon[38] and the number of possible unoccupied molecular orbitals depends on the local electronic structure of the excited atom, NEXAFS spectra were used to differentiate between PMMA and PI or PEP so that polymer-specific absorption images of the blends could be generated without ex situ staining.

The physical properties of the cryomilled PEP/PMMA and PI/PMMA blends were examined by Izod impact tests performed at ambient temperature on a Tinius-Olsen model 92T plastics impact tester modified to accept 10 mm samples. Samples for impact testing were prepared by first compacting about 1.6 g of powder into a disk measuring 25 mm in diameter at 20 °C and 88 MPa for 5 min. These disks were melt-pressed into squares with minimal pressure at ca. 40 °C above the glass transition temperature (T_g) of PMMA after milling time t_m (T_g values ranged between 60 and 120 °C, as determined by differential scanning calorimetry of cryomilled PMMA homopolymer[34]) for 5 min and then quenched as before. Resultant plaques measured 25 mm × 25 mm × 2 mm and were cut into "matchsticks" measuring 2 mm × 4 mm

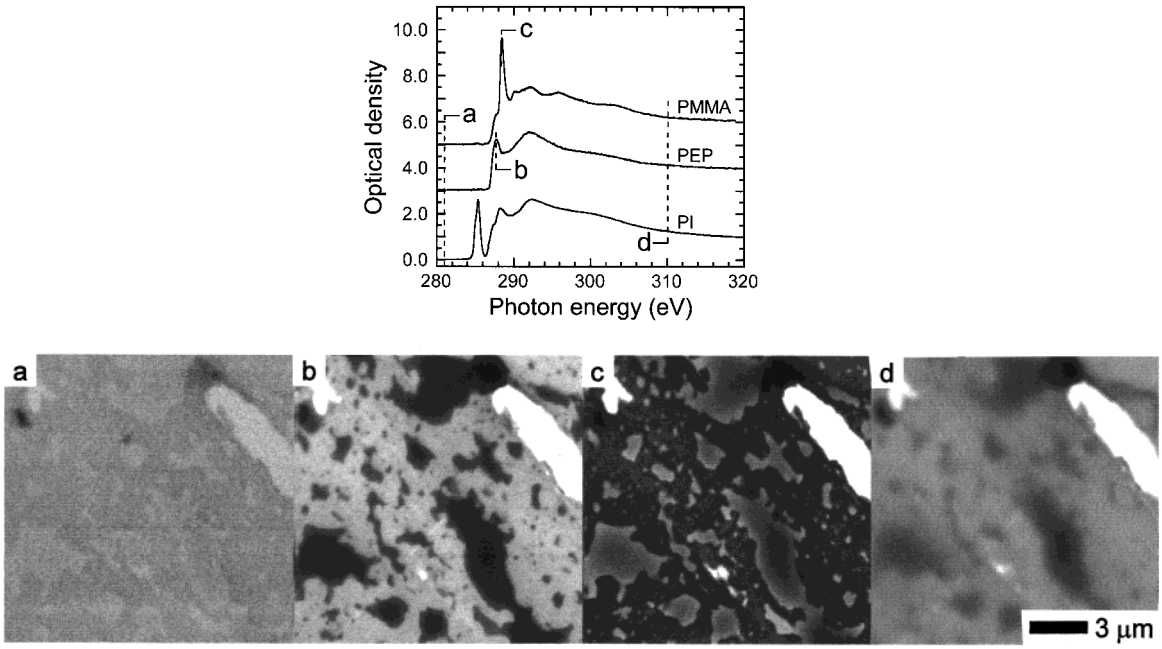

Figure 2. Mass-normalized NEXAFS absorption spectra of PMMA, PEP, and PI shifted vertically to facilitate comparison. By exploiting differences in X-ray absorption cross sections, chemically specific images can be obtained without staining, as shown in parts a−d. STXM images are obtained from a 25/75 PEP/PMMA blend (cryomilled for 5 h and melt-pressed at 125 °C) at four photon energies (in eV): (a) 281.0 (pre-edge), (b) 288.0 (PEP dark), (c) 288.4 (PMMA dark), and (d) 310.0 (carbon optical density/thickness). White areas identify holes in the specimen.

× 25 mm with a diamond saw. Each matchstick was placed 5 mm deep into the sample clamp of the impact tester and oriented so that the striker contacted the 2 mm side of the matchstick and fracture occurred along the 4 mm side. A torque of 60 N cm (330 N of force or 33 MPa of pressure) was applied to the sample clamp. After initial fracture, the remaining matchstick was tested two additional times until it became unusably short. Approximately 15 measurements were conducted per sample with any obviously erroneous points discarded. Optical properties of PI/PMMA blends were measured by light microscopy. The fraction of transmitted light through blends cryomilled for 5 h was deduced from the ratio of the average transmission intensity to that of an unoccupied field of view.

Results and Discussion

Blend Morphology. Characterization of blend morphology by STXM requires that an appropriate X-ray energy for phase differentiation in each polymer pair be identified. Two such energies are evident upon close comparison of the NEXAFS homopolymer spectra presented in Figure 2. In this figure, the C K-edge NEXAFS spectra obtained from PMMA, PEP, and PI are mass-normalized so that each spectrum is set to 1.0 at 319.0 eV and 0.0 at 280.0 eV. Moreover, the spectra for PMMA and PEP are shifted vertically to facilitate comparison. As discussed elsewhere,[39] the most prominent spectral features in NEXAFS spectra occur due to unsaturation within polymers. The PMMA spectrum exhibits a sharp peak at 288.4 eV due to excitation of bonds corresponding to the C═O functionality, while the PI spectrum displays a peak at 285.0 eV due to excitation of C═C bonds. In contrast, the PEP spectrum possesses a relatively broad peak at 288.0 eV (which is common for polyolefins[39,40]), but no sharp peak. Thus, the constituent polymers in each blend can be identified through judicious choice of photon energy, as illustrated in the micrographs included in Figure 2.

These micrographs of an unstained 25/75 PEP/PMMA blend cryomilled for 5 h and pressed at 125 °C were acquired at energies (in eV) of 281.0 (Figure 2a), 288.0 (Figure 2b), 288.4 (Figure 2c), and 310.0 (Figure 2d). As indicated in the NEXAFS composite spectrum, the micrograph at 281.0 eV corresponds to an energy below the C K-edge and reveals the presence of non-carbonaceous elements. In this case, PMMA appears slightly darker than PEP due to its oxygen content. At 288.0 eV, PEP absorbs more X-rays and thus appears dark relative to PMMA. This contrast is reversed in the image acquired at 288.4 eV so that PMMA appears dark. Figure 2d, obtained at 310.0 eV, is not chemically specific and primarily represents a carbon optical density/thickness image. At this energy, PEP appears dark since it bulges slightly in the thin section, thereby creating thick areas. Unchanging bright areas in Figure 2 (and later) correspond to holes in the section. A similar series of images (not shown here) is obtained for the PI/PMMA blends when a photon energy of 285.0 eV is utilized to identify PI. Throughout the remainder of this work, STXM images are provided at an energy where the rubber appears dark (288.0 eV for PEP or 285.0 eV for PI).

The morphologies of several 25/75 PEP/PMMA blend series are shown in Figure 3, in which the STXM images correspond to an energy of 288.0 eV so that PEP appears dark. The blends have been cryomilled for 4 different t_m (in h)—1 (top row; Figure 3a−c), 3 (second row; Figure 3d−f), 5 (third row; Figure 3g−i), and 8 (bottom row; Figure 3j−l)—and subsequently pressed at three different temperatures (in °C)—20 (first column; Figure 3a,d,g,j), 125 (second column; Figure 3b,e,h,k), and 200 (third column; Figure 3c,f,i,l). For the blends pressed at ambient temperature, the PEP is able to flow between glassy PMMA particles and subsequently outlines them. In the blend cryomilled for 1 h (Figure 3a), the PMMA particles measure 0.2−3 μm in size and possess irregular shapes. As t_m increases (as in Figure 3d,g), the PMMA particles are seen to decrease in size: the

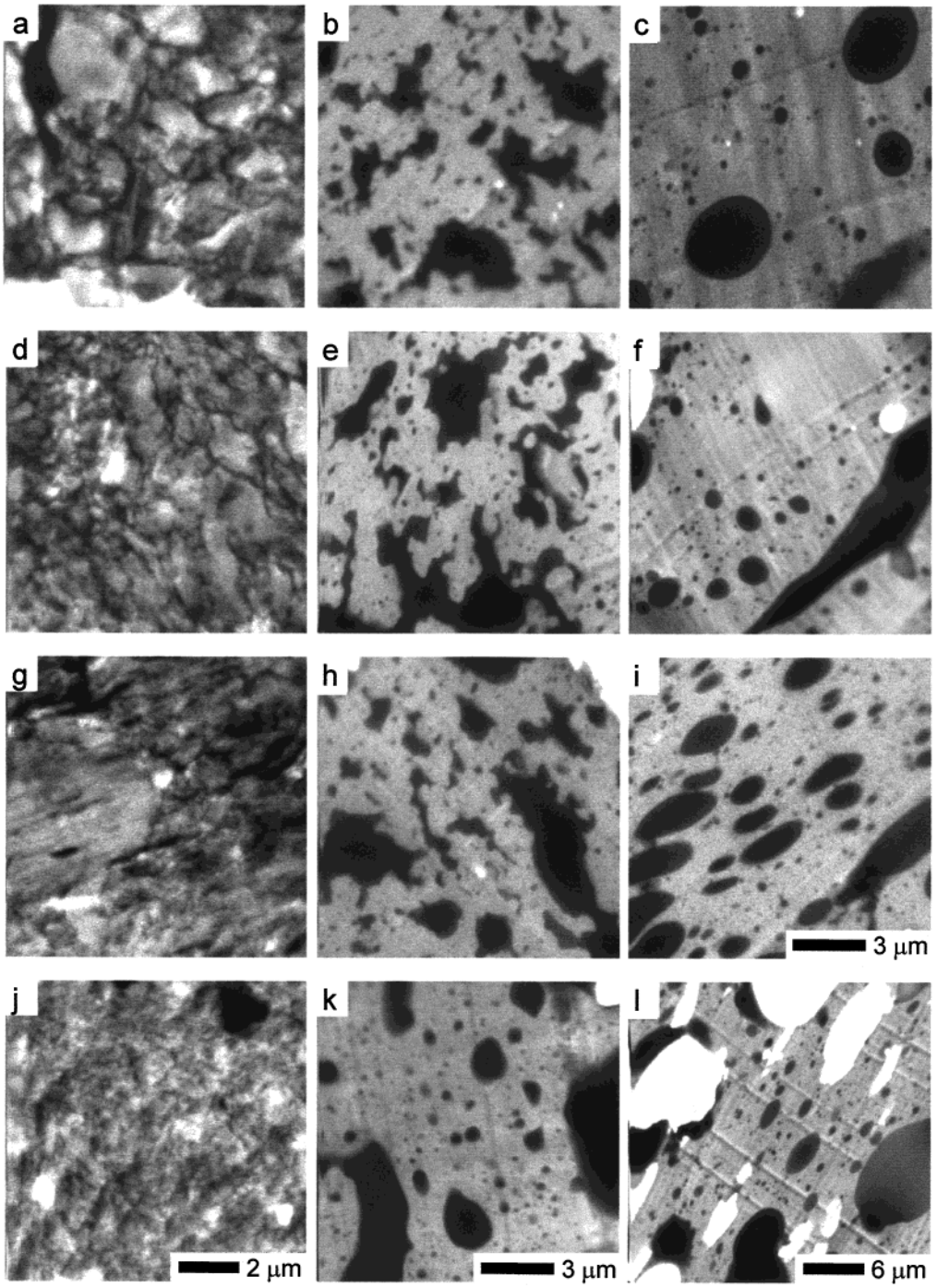

Figure 3. STXM images acquired at 288.0 eV (PEP dark) from 25/75 PEP/PMMA blends cryomilled for different t_m (in h): 1 (a−c), 3 (d−f), 5 (g−i), and 8 (j−l). The columns correspond to different pressing temperatures (in °C): 20 (column 1: a, d, g, and j), 125 (column 2: b, e, h, and k), and 200 (column 3: c, f, i, and l). The scale markers for the images in columns 1 and 2 are provided in parts j and k, respectively, while the scale marker for images (parts c, f, and i) in column 3 is shown in part i. The image in part l is presented at a different magnification.

particles are about 1 μm across after 3 h of cryomilling (Figure 3d) and 0.5 μm across in the blend cryomilled for 5 h (Figure 3g). After 8 h of milling (Figure 3j), the outlining of PMMA by PEP appears incomplete, but demonstrates that the PMMA domain size is reduced to ca. 300 nm. These results indicate that PEP can be highly dispersed within PMMA by mechanical alloying.

The images obtained from the samples pressed at 125 and 200 °C reveal the blend morphologies in the melt. In blends processed at 125 °C, PEP-rich domains, ranging in size from about 0.2 to 5 μm, reside in a continuous PMMA matrix. The PEP domains in blends cryomilled for 5 h or less possess irregular shapes, suggesting that the nonequilibrium morphology imparted by mechanical alloying is retained in these blends. After 5 h of cryomilling, the T_g of PMMA is measured[34] to be 98 °C, in which case the viscosity of the PMMA matrix at 125 °C remains sufficiently high to inhibit substantial PEP migration. Further reduction of the T_g to 91 °C after 8 h of cryomilling, however, imparts the PEP chains in the blend pressed at 125 °C (Figure 3K) with sufficient mobility to diffuse and form domains that appear spheroidal (or elliptical due to flow during pressing).[41] Such evolution is consistent with

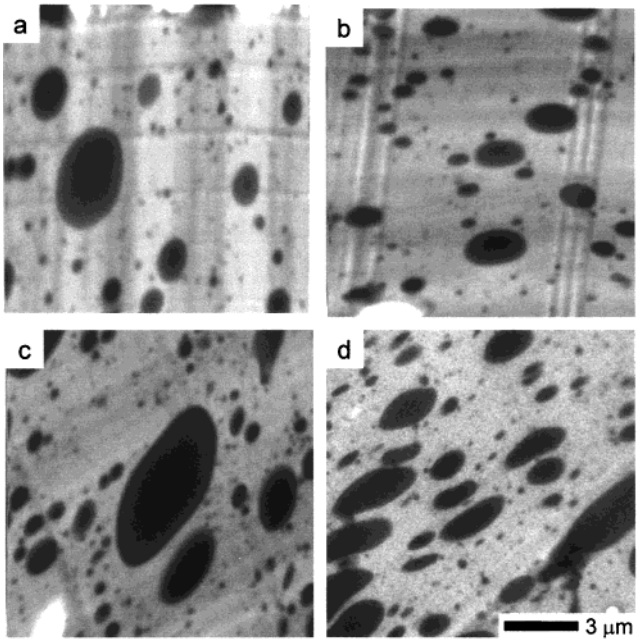

Figure 4. STXM images acquired from PEP/PMMA blends cryomilled for 5 h and melt-pressed at 200 °C with different concentrations of PEP (in wt %): (a) 10, (b) 15, (c) 20, and (d) 25. The population of PEP domains (dark) increases with increasing PEP concentration.

minimization of the surface area of the PEP phase, as well as the free energy of the blend. Similar behavior is evident in the images acquired from blends cryomilled for 5 h or less and melt-pressed at 200 °C. Another interesting feature of these images is the increase in the number of small (<1 μm) PEP domains with increasing t_m, suggesting that large domains break up under these conditions. After 8 h of cryomilling, the melt-pressed PEP/PMMA blend (Figure 3l) undergoes significant PEP agglomeration (note the magnification change). In this image, one large intact PEP domain is accompanied by numerous holes where PEP is believed to have flowed from the thin section. While all the images in Figure 3 confirm the immiscibility of PEP and PMMA, Figure 3l provides an indication of the rapid rate at which domain coalescence can occur in such polymer blends, which are mixed at nanoscale dimensions and subjected to postprocessing.

Another variable of interest in PEP/PMMA blends produced by mechanical alloying is the concentration of PEP. Figure 4 displays a series of STXM images collected under the same conditions as those in Figure 3 and showing the morphologies of PEP/PMMA blends cryomilled for 5 h, melt-pressed at 200 °C and containing different levels of PEP (in wt %): 10 (Figure 4a), 15 (Figure 4b), 20 (Figure 4c), and 25 (Figure 4d). As anticipated from the images presented in Figure 3 (third column), each of these blends exhibits a smooth domain morphology in which PEP is dispersed within a PMMA matrix. As the concentration of PEP is increased, the population of PEP domains is seen to increase, but the size distribution of PEP domains in these images appears to be insensitive to relatively large changes in PEP content. Attempts to characterize the morphologies of blends with lower PEP concentration or pressed at temperatures below 200 °C have proven unsuccessful due to difficulty associated with sample brittleness.

To ascertain the effect of polymer chemistry on the blends produced in this work by cryogenic mechanical alloying, complementary PI/PMMA blends have also been prepared. Previous analysis of the effect of high-energy ball milling on PI has demonstrated that this homopolymer undergoes chemical cross-linking during cryomilling.[34] This difference between PI and PEP is expected a priori to have a dramatic effect on the morphology and phase stability of PI/PMMA blends. Figure 5 shows STXM images acquired from nominally 25/75 PI/PMMA blends acquired at 285.0 eV, at which PI absorbs X-rays and appears dark. [Note that, at short t_m (ca. 1 h), the blend compositions deviate somewhat from the targeted 25/75 PI/PMMA blend composition due to incomplete incorporation of PI within the PMMA matrix.] These blends have been cryomilled for different t_m (in h)—1 (Figure 5a–c), 5 (Figure 5d–f), and 10 (Figure 5g–i)—and consolidated at 20 °C (first column; Figure 5a,d,g), 125 °C (second column; Figure 5b,e,h), and 200 °C (third column; Figure 5c,f,i). The morphologies of the blends consolidated at ambient temperature appear similar to those observed in the PEP/PMMA blends prior to melt-pressing. As in Figure 3, the PI flows around and delineates the PMMA particles, which decrease in size with increasing t_m. After 1 h of cryomilling (Figure 5a), the PMMA particles measure less than 2 μm across and subsequently decrease to less than 300 nm in the blend milled for 10 h (Figure 5g).

Differences in the phase behavior between PI/PMMA and PEP/PMMA blends become readily apparent after postprocessing the blends at elevated temperatures.[41] Recall from Figures 3 and 4 that the PEP/PMMA blends exhibit relatively large PEP domains (>3 μm) due to phase coarsening upon melt-pressing. As seen in the STXM images presented in Figure 5, the PI domains in blends consolidated at 125 (Figure 5b,e,h) and 200 °C (Figure 5c,f,i) remain considerably smaller (<1 μm) and, in some cases, become highly interconnected to form a semicontinuous network within the PMMA matrix. At 125 °C, the blend milled for 10 h (Figure 5h) shows an almost identical morphology to that observed in the blend pressed at 20 °C (Figure 5g), indicating that temperature has little effect on blend morphology. With additional heating, however, the morphology clearly evolves. The PI in the blend cryomilled for 1 h and subsequently processed at 200 °C (Figure 5c), for example, forms small isolated dispersions in the PMMA matrix with little evidence of interconnectivity. Similarly, the blend cryomilled for 5 h (Figure 5f) also consists of isolated PI dispersions within the PMMA matrix, although these dispersions are more asymmetric and larger (measuring up to 4 μm along the long axis) relative to those visible in Figure 5c. According to Figure 5i, an interconnected PI morphology with locally isolated regions of PMMA develops in the PI/PMMA blend cryomilled for 10 h.

Closer examination of PI/PMMA blends by TEM (Figure 6) reveals that blends pressed at ambient temperature (Figure 6a) initially possess a high degree of dispersion at nanoscale dimensions, with PMMA-rich regions ranging from 10 to 500 nm across. In this and other TEM images, the PI appears electron-opaque (dark) due to selective staining with OsO_4. When consolidated at 125 °C (Figure 6b), the PI forms small isolated domains (measuring up to 30 nm across), as well as interconnected regions with PMMA inclusions. The blend milled for 10 h undergoes far less coarsening than its PEP/PMMA analogue upon melt-pressing at 200 °C (Figure 6c) and retains a semicontinuous nanos-

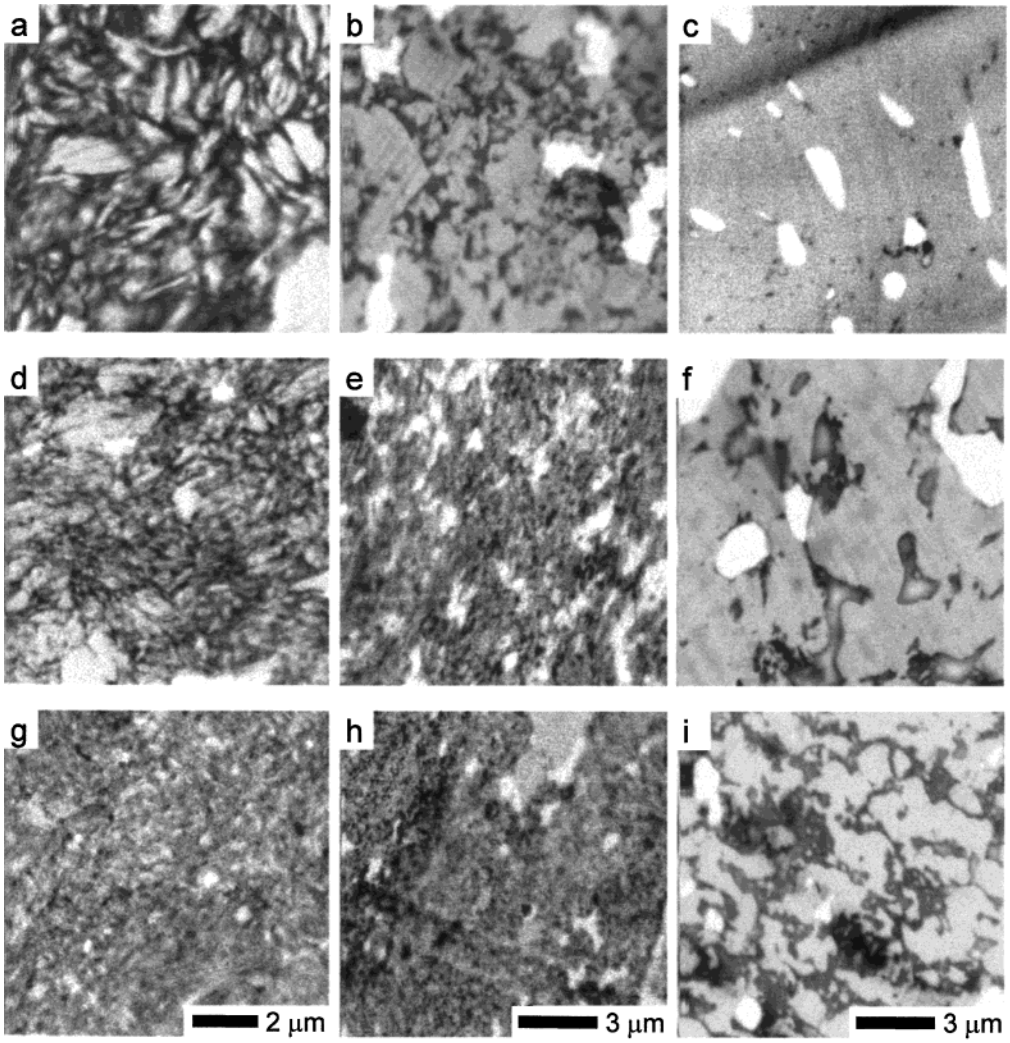

Figure 5. STXM images acquired at 285.0 eV (PI dark) from 25/75 PI/PMMA blends cryomilled for different t_m (in h): 1 (a−c), 5 (d−f), and 10 (g−i). The columns correspond to different pressing temperatures (in °C): 20 (column 1: a, d, and g), 125 (column 2: b, e, and h), and 200 (column 3: c, f, and i). As t_m increases, the morphological features decrease in size. Relative to the analogous PEP/PMMA blends (see Figure 3), the PI phase consists of substantially finer domains at higher pressing temperatures and, in some cases, appears to form a semicontinuous nanoscale network.

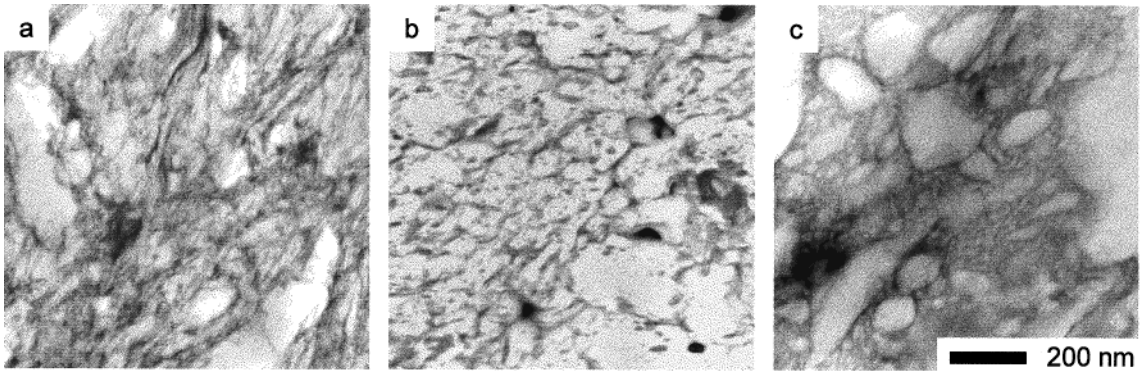

Figure 6. TEM micrographs of 25/75 PI/PMMA blends cryomilled for 10 h and pressed at three different temperatures (in °C): (a) 20, (b) 125, and (c) 200. Blends have been stained by the vapor of OsO_4(aq) so that the PI appears electron-opaque (dark). All of these images reveal microstructural features as small as 10 nm, which confirms that an extremely fine polymer dispersion is possible by solid-state mechanical alloying.

cale PI network in which the smallest resolvable PI features are about 5 nm across and PMMA-rich inclusions measure as small as 10 nm across. The observation that the connectivity of the PI phase remains after melt-pressing implies that, under the preparation conditions employed here, the morphology of this blend is not strongly dependent on pressing temperature, which is consistent with the expectation that the PI is chemically cross-linked.

Figure 7 shows STXM images of PI/PMMA blends with varying PI content cryomilled for 5 h and melt-pressed at 200 °C. These images, acquired at 285.0 eV, at PI concentrations (in wt %) of 10 (Figure 7a), 15 (Figure 7b), 20 (Figure 7c), and 25 (Figure 7d), reveal

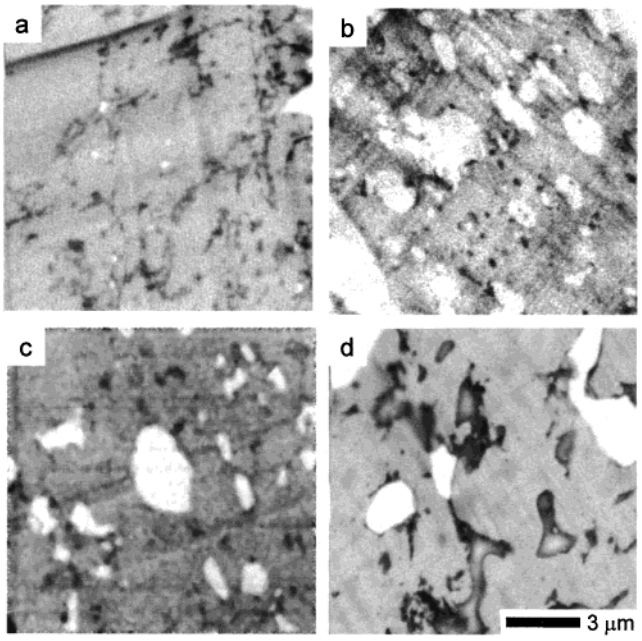

Figure 7. STXM images acquired from PI/PMMA blends (cryomilled for 5 h and melt-pressed at 200 °C) with different concentrations of PI (in wt %): (a) 10, (b) 15, (c) 20, and (d) 25. These images demonstrate that the PI domains become larger and more numerous as the PI content increases.

that PI forms domains within a continuous PMMA matrix, and that the PI domains increase in size and frequency as the PI content increases. As in the case of the PEP/PMMA blends (Figure 3), open (white) areas in the STXM images provided in Figure 7 correspond to regions out of which PI in the thin sections flowed. In the blend with 10 wt % PI (Figure 7a), PI-rich domains are seen to remain relatively uniform (in terms of size and size distribution) below 1 μm. As the PI concentration is increased to 25 wt % (Figure 7d), the PI domains approach 3 μm in size and exhibit a larger and less uniform size distribution within the PMMA matrix. On the basis of the morphological results presented thus far, the PEP/PMMA blends are anticipated to possess different mechanical properties from the PI/PMMA blends under identical processing and composition conditions. The next section compares the impact strength of these blend series.

Mechanical Properties. The effect of mechanical alloying on the mechanical properties of PEP/PMMA and PI/PMMA blends has been examined here through the use of Izod impact testing. Previous work[34] has shown that the impact strength of PMMA is directly proportional to $\bar{M}_n$ over the interval 20 000 < $\bar{M}_n$ < 100 000. Since $\bar{M}_n$ decreases substantially with increasing t_m, a reduction in the impact strength of the PMMA matrix is expected to coincide with an increase in t_m. Evaluation of the contribution of PEP or PI to the impact strength of PMMA therefore requires attention to this consideration. The variation of impact strength with t_m for PEP/PMMA and PI/PMMA blends cryomilled up to 10 h is displayed in Figure 8. Included for comparison in this figure are data collected from cryomilled PMMA. Inspection of these data reveals several trends. First, an increase in t_m yields a more pronounced reduction in the impact strength of the PEP/PMMA blends than in the analogous PI/PMMA blends. Although the blends with PEP possess a higher initial strength than the blends with PI, the PI/PMMA blends

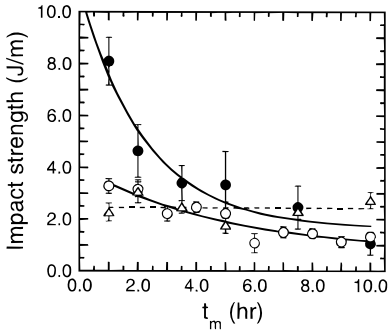

Figure 8. Impact strength as a function of t_m for 25/75 PEP/PMMA blends (○), 25/75 PI/PMMA blends (△), and pure PMMA (●) milled at cryogenic temperatures. The solid lines are exponential fits to the PEP/PMMA and PMMA data,[34] whereas the dashed horizontal line is a linear regression to the PI/PMMA data. Error bars denote one standard deviation in the data. Note that the PI/PMMA blends cryomilled in excess of ca. 8 h become tougher than pure PMMA subjected to identical cryomilling conditions.

exhibit higher impact strength after a few hours of cryomilling. In addition, the PEP/PMMA blends are always less tough than pure PMMA milled for the same t_m, whereas the PI blends become more fracture resistant than pure PMMA after ca. 8 h of cryomilling. (It must be recognized, however, that the magnitude of the blend impact strength under these conditions remains significantly below the strength of the as-received PMMA.) While the time-dependent change in impact strength for the PEP/PMMA blends follows the same exponential reduction as pure PMMA,[34] the impact strength of the PI/PMMA blends remains nearly invariant with respect to t_m, which (in the absence of any other observed differences between cryomilled PEP and PI) is once again attributed to the chemical cross-linking of PI.

Several criteria must be satisfied for successful rubber toughening of a thermoplastic.[27,28] The two that most seriously affect the measured impact strength are (i) the size of the rubber domains and (ii) the interfacial tension between the rubber and matrix. Conventional toughening requires that the rubber domains must be discrete and measure on the same size scale as the fracture front. Likewise, interfacial adhesion must expedite the transfer of stress energy to rubbery domains, wherein it can be dissipated. Consideration of these criteria in conjunction with the morphological characteristics presented thus far can be used to explain the impact behavior of the blends produced in this study. Previous efforts have established that the optimum size for rubber dispersions within PMMA lies between 200 and 300 nm.[42−44] Analysis of the STXM images obtained from the PEP/PMMA blends pressed at 125 °C (see Figure 3) reveals that, while PEP domains on this size scale exist, domains as large as 5 μm across are also present. Such large domains serve to weaken the matrix. In addition, the morphologies of PEP/PMMA blends undergo substantial phase separation upon heating, which implies that little interfacial adhesion exists between PEP and PMMA. With these shortcomings in mind, many of the heat-treated PEP/PMMA blends produced here can be envisaged as a PMMA matrix with nearly 25% voids, since the large PEP domains do not serve to dissipate impact energy. The overall reduction in toughness is also related to the decrease in PMMA $\bar{M}_n$. Similar criticisms apply to the PI/PMMA blends with the principal difference that the PI domains are

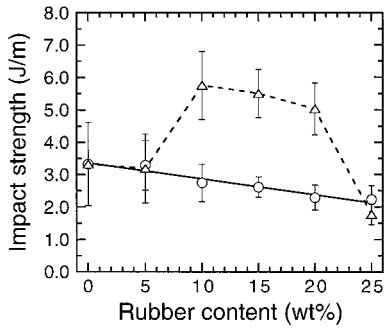

Figure 9. Variation of impact strength with rubber concentration for PEP/PMMA and PI/PMMA blends cryomilled for 5 h. The symbols are the same as those defined in the caption of Figure 8. The solid line denotes a linear regression of the PEP/PMMA data, while the dashed line connects the PI/PMMA data points. Note the increase in impact strength between 10 and 20 wt % PI.

chemically linked to form a network rather than large distinct particles. The invariance of impact strength in the PI/PMMA blends with t_m therefore appears to depend more on the cross-linking of PI and the nanostructure produced (see Figure 6) than on the $\bar{M}_n$ decrease of the PMMA matrix (relative to pure PMMA). It should be noted at this juncture that the t_m-dependent $\bar{M}_n$ reduction of PMMA in PEP/PMMA and PI/PMMA blends may differ somewhat from that of pure PMMA.

Another important variable to be considered in rubber toughening is the amount of rubber incorporated into a blend. If an insufficient quantity of rubber is utilized, impact toughening will be negligible, while an excess of rubber will serve to degrade the strength of the blend.[30] To determine if the blends produced here by mechanical alloying follow these guidelines, the impact strength of PEP/PMMA and PI/PMMA blends cryomilled for 5 h is presented as a function of rubber concentration in Figure 9. When the two sets of data are compared, no improvement or difference is observed for either blend series up to 5 wt % rubber. Between 10 and 20 wt % rubber, the PEP/PMMA blends undergo a gradual reduction in impact strength, whereas the PI/PMMA blends exhibit a marked increase in impact strength (by more than 100%, relative to that of the analogous PEP/PMMA blend). At 25 wt % rubber, the impact strengths of the PEP/PMMA and PI/PMMA blends are equal within experimental error, indicating that the type of rubber employed at this level has little effect on impact strength. The trends apparent in Figure 9 can be analyzed in terms of blend morphology as before. The PEP domains (see Figure 4) are relatively large and dispersed, which makes them ineffective for rubber toughening. The PI domains in blends with 10−20 wt % PI are, with few exceptions, about 500 nm in diameter, which makes them ideal (in terms of size) for rubber-toughening PMMA. When the concentration of PI reaches 25 wt %, the PI-rich domains are too large to promote toughening, and the blend becomes correspondingly less fracture resistant.

Optical Properties. Perhaps the most useful property of PMMA is its optical clarity, which constitutes a primary design consideration in the majority of its end-use applications. Any successful attempt to toughen PMMA must therefore maintain the inherent optical clarity of PMMA as much as possible. In the case of the mechanically alloyed PEP/PMMA blends, the large PEP domains scatter visible light, and the samples appear completely opaque to the unaided eye. The PI/PMMA blends, however, possess varying degrees of transparency, depending on composition. This variation in transparency is displayed in Figure 10 by a series of optical (transmission) micrographs obtained from PI/PMMA blends cryomilled for 5 h with different PI concentrations (in wt %)—0 (Figure 10a), 5 (Figure 10b), 10 (Figure 10c), and 15 (Figure 10d). In each of these micrographs, the left-hand side is the reference transmitted intensity (without a sample present), and the right-hand side shows the intensity of light transmitted through a 2 mm thick specimen. Examination of these micrographs confirms that the optical transparency of the blends decreases with increasing rubber content.

To quantitate the transparency of each blend, the average transmitted intensities measured from a specimen and its reference have been calculated from the areas outlined in Figure 10a. Dividing the intensity transmitted through the specimen by the reference intensity under the same illumination conditions yields the fraction of light transmitted through the specimen. This fraction (f) is normalized with respect to that of pure, cryomilled PMMA ($f = 0.80$) to generate a relative measure of blend transparency, which is provided as a function of PI concentration in Figure 10e. (Similar analysis of as-received PMMA yields $f = 0.83$.) Figure 10e reveals that, at PI loadings in excess of 5 wt %, the blend transparency decreases exponentially with increasing PI concentration. Thus, mechanical alloying of PI and PMMA at PI concentrations needed to improve impact resistance does not yield transparent blends produced at the t_m examined here (5 h). At 10 wt % PI, the optical clarity is degraded by 57%, which is consistent with the morphology of this blend. According to Figure 7a, the PI domains primarily measure below 500 nm in size, with only a few large enough to be optically interfering. As the content of PI increases, the domains grow larger and more prevalent, and their ability to scatter light improves, thereby producing opaque blends. Production of PI/PMMA blends possessing an acceptable impact strength and transparency therefore requires optimization with respect to design considerations such as t_m and PI concentration.

Conclusions

In this study, physical blends of PMMA with either PI or PEP have been produced by mechanical alloying performed at cryogenic temperatures. X-ray and electron microscopies have been utilized to examine the morphological characteristics of these blends. The morphologies of blends consolidated at ambient temperature in both blend series reveal that (i) a high degree of polymer dispersion is achieved upon solid-state mechanical alloying, and (ii) the degree of dispersion improves with milling time and remains largely unaffected by variation in PEP or PI concentration. When blend powders are postprocessed above the T_g of the PMMA matrix, however, the morphological evolution of PEP-containing blends differs significantly from blends with PI. The inherent immiscibility between PEP and PMMA promotes gross phase separation, resulting in the formation of relatively large PEP domains. This phase separation occurs at shorter times for PEP/PMMA blends milled for longer times, which coincides with a more pronounced reduction in $\bar{M}_n$ of PMMA and a corresponding reduction in the viscosity of the matrix. While phase separation also occurs in molten PI/PMMA blends, the rate of separation is substantially less than

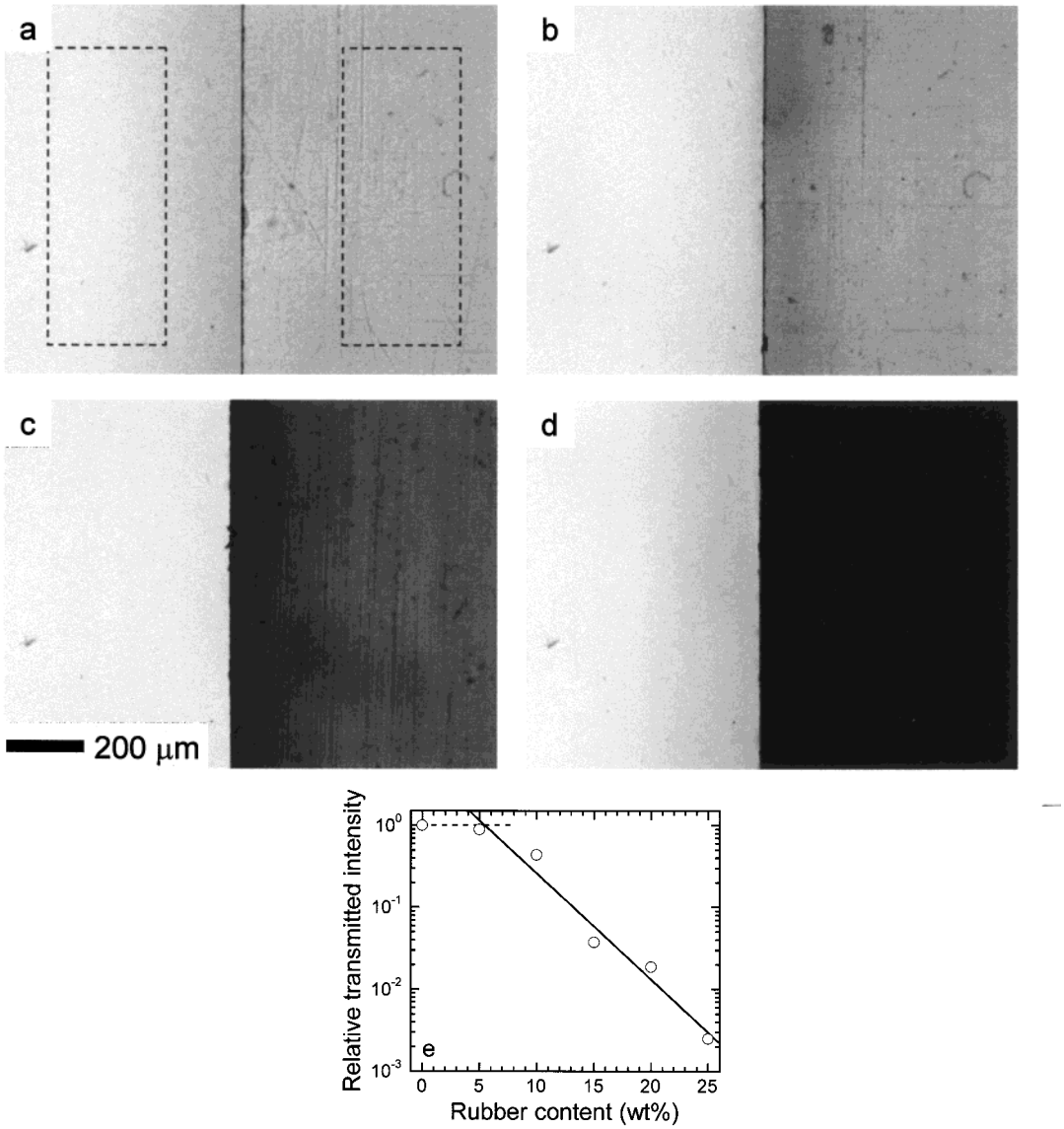

Figure 10. Optical micrographs of PI/PMMA samples cryomilled for 5 h with different PI concentrations (in wt %): (a) 0, (b) 5, (c) 10, and (d) 15. The left side of each image is unobscured. The relative transmitted intensity, calculated from the ratio of average intensities in the boxed regions shown in part a and normalized with respect to pure PMMA, is presented as a function of PI concentration in part e. The solid line is an exponential fit to the data beyond 5 wt % PI, and the dashed line identifies a relative intensity of unity.

that observed in analogous PEP/PMMA blends. Moreover, PI forms semicontinuous networks that contain PMMA inclusions, rather than large, dispersed domains. This morphological development is consistent with the expected cross-linking of PI due to high-energy milling but provides no discernible evidence for the chemical coupling of PI with PMMA.

In addition to morphological characterization, Izod impact testing has been performed on these blends to discern the variation of impact strength with milling time and rubber composition. For blends with 25 wt % rubber, the toughness of the PEP/PMMA blends is found to decrease monotonically with increasing milling time, whereas the impact strength of PI/PMMA blends is nearly independent of milling time. While all the blends tested possess impact strengths significantly below that of the as-received PMMA, the PI/PMMA blends are more fracture resistant than the pure PMMA after cryomilling times of approximately 8 h. Variation in rubber concentration yields a difference in impact strength between PEP/PMMA and PI/PMMA blends. Blends with PEP exhibit no measurable change in impact strength below 10 wt % PEP, but undergo a gradual reduction in impact strength with increasing rubber concentration above 10 wt % PEP. The PI-containing blends, however, exhibit a marked improvement in impact strength between 10 and 20 wt % PI. The failure of either rubber to significantly toughen PMMA in these blends is attributed to insufficient rubber dispersion size and interfacial adhesion. The optical clarity of several PI/PMMA blends has also been measured, and the relative transparency has been found to decrease exponentially with increasing PI concentration. Blends with PEP are, however, completely opaque at all blend compositions investigated.

While the results obtained here clearly reveal that rubber toughening of PMMA by cryogenic mechanical alloying yields inferior blends (relative to those produced by current commercial methods) with respect to mechanical and optical properties, this study confirms that solid-state blending of polymeric materials can yield nanoscale dispersions of immiscible polymers. The final

morphological characteristics and physical properties of these blends are found to depend strongly on subsequent processing of the cryomilled powders. On the basis of the results presented in this work, it is anticipated that judicious substitution of more degradation-resistant (less brittle) thermoplastic polymers, such as those synthesized via condensation routes, for PMMA will yield blends possessing more promising properties, as well as equally exciting morphologies.

Acknowledgment. X-ray microscopy data were collected using the Stony Brook STXM instrument developed by the group of J. Kirz and C. Jacobsen at SUNY Stony Brook, with financial support from the Office of Biological and Environmental Research, U.S. DOE under Contract DE-FG02-89ER60858, and NSF under Grant DBI-960-5045. S. Spector and C. Jacobsen of SUNY Stony Brook and D. Tennant of Lucent Technologies developed the zone plates with support from NSF under Grant ECS-951-0499. An NSF Young Investigator Award (DMR-945-8060) supports H. A. and A. P. S. We thank D. A. Winesett and S. G. Urquhart for technical assistance.

References and Notes

(1) Macosko, C. W.; Guegan, P.; Khandpur, A. K.; Nakayama, A.; Marechal, P.; Inoue, T. *Macromolecules* **1996**, *29*, 5590.
(2) Utracki, L. A. *Polymer Alloys and Blends*; Hanser: Berlin, 1990. See also: Utracki, L. A. *Commercial Polymer Blends*; Kluwer Academic: Dordrecht, The Netherlands, 1998.
(3) Feng, Y.; Weiss, R. A.; Han, C. C. *Macromolecules* **1996**, *29*, 3925.
(4) Bouilloux, A.; Ernst, B.; Lobbrecht, A.; Muller, R. *Polymer* **1997**, *38*, 4775.
(5) Ahn, D.; Khait, K.; Petrich, M. A. *J. Appl. Polym. Sci.* **1995**, *55*, 1431.
(6) Nesarikar, A. R.; Carr, S. H.; Khait, K.; Mirabella, F. M. *J. Appl. Polym. Sci.* **1997**, *63*, 1179.
(7) Furgiuele, N.; Lebovitz, A. H.; Khait, K.; Torkelson, J. M. *Macromolecules*, **2000**, *33*, 225.
(8) Pan, J.; Shaw, W. J. D. *Microstruct. Sci.* **1993**, *20*, 351.
(9) Shaw, W. J. D.; Pan, J.; Growler, M. A. In *Proceedings of the 2nd International Conference on Structural Applied Mechanical Alloying*; DeBarbadillo, J. J., Fores, F. H., Schwarz, R., Eds.; ASM International: Materials Park, OH, 1993; p 431.
(10) Castricum, H. L.; Yang, H.; Bakker, H.; Deursen, J. H. V. *Mater. Sci. Forum* **1997**, *235*−*238*, 211.
(11) Farrell, M. P.; Kander, R. G.; Aning, A. O. *J. Mater. Synth. Proc.* **1996**, *4*, 1996.
(12) Font, J.; Muntasell, J.; Cesari, E. *Mater. Res. Bull* **1999**, *34*, 157.
(13) Ishida, T. *J. Mater. Sci. Lett.* **1994**, *13*, 623.
(14) Koch, C. C. In *Materials Science and Technology*; Cahn, R. W., Ed.; VCH: Weinheim, Germany, 1991; Vol. 15, p 583.
(15) Benjamin, J. S. *Metall. Trans.* **1970**, *1*, 2943.
(16) Benjamin, J. S. In *New Materials by Mechanical Alloying Techniques*; Arzt, E., Schultz, L., Eds.; Deutsche Gesellschaft für Metallkunde: Oberursel, Germany, 1989; pp 1−18.
(17) Koch, C. C.; Cavin, O. B.; McKamey, C. G.; Scarborough, J. O. *Appl. Phys. Lett.* **1983**, *43*, 1017.
(18) Lu, L.; Lai, M. O. *Mechanical Alloying*; Kluwer Academic: Norwell, MA, 1998.
(19) Murty, B. S.; Ranganathan, S. *Int. Mater. Rev.* **1998**, *43*, 101.
(20) Tang, J.; Zhao, W.; Li, L.; Falster, A. U.; Jr., W. B. S.; Zhou, W. L.; Ikuhara, Y.; Zhang, J. H. *J. Mater. Res.* **1996**, *11*, 733.
(21) Tsukushi, I.; Yamamuro, O.; Suga, H. *Thermochim. Acta* **1992**, *200*, 71.
(22) Font, J.; Muntasell, J.; Cesari, E.; Pons, J. *J. Mater. Res.* **1997**, *12*, 3254.
(23) Fukunaga, T.; Nagano, K.; Mizutani, U.; Wakayama, H.; Fukushima, Y. *J. Non-Cryst. Solids* **1998**, *232*−*234*, 416.
(24) Balik, C. M.; Bai, C.; Koch, C. C.; Spontak, R. J.; Saw, C. K. *Mater. Res. Soc. Symp. Proc.* **1997**, *461*, 39.
(25) Smith, A. P.; Bai, C.; Ade, H.; Spontak, R. J.; Balik, C. M.; Koch, C. C. *Macromol. Rapid Commun.* **1998**, *19*, 557.
(26) Smith, A. P.; Spontak, R. J.; Ade, H.; Smith, S. D.; Koch, C. C. *Adv. Mater.* **1999**, *11*, 1277.
(27) Bucknall, C. B. *Toughened Plastics*; Applied Science Publishers: London, 1977.
(28) Partridge, I. K. In *Multicomponent Polymer Systems*; Miles, I. S., Rostami, S., Eds.; Longman Scientific and Technical: Essex, England, 1992; p 149.
(29) Walker, I.; Collyer, A. A. In *Rubber Toughened Engineering Plastics*; Collyer, A. A., Ed.; Chapman & Hall: London, 1994; p 29.
(30) Bucknall, C. B. In *The Physics of Glassy Polymers*, 2nd ed.; Haward, R. N., Young, R. J., Eds.; Chapman and Hall: New York, 1997.
(31) Vazquez, F.; Schneider, M.; Pith, T.; Lambla, M. *Polym. Int.* **1996**, *41*, 1.
(32) Lovell, P. A. *Trends Polym. Sci.* **1996**, *4*, 264.
(33) Wrotecki, C.; Heim, P.; Gaillard, P. *Polym. Eng. Sci.* **1991**, *31*, 213.
(34) Smith, A. P.; Shay, J. S.; Spontak, R. J.; Balik, C. M.; Ade, H.; Smith, S. D.; Koch, C. C. *Polymer*, in press.
(35) Feser, M.; Carlucci-Dayton, M.; Jacobsen, C.; Kirz, J.; Neuhäusler, U.; Smith, G.; Yu, B. In *X-ray Microfocusing: Applications and Techniques*; McNulty, I., Ed.; Society of Photo-Optical Instrumentation Engineers SPIE: Bellingham, WA, 1998; Vol. 3449, p 19.
(36) Spector, S.; Jacobsen, C.; Tennant, D. *J. Vac. Sci. Technol. B* **1997**, *15*, 2872.
(37) Ade, H.; Zhang, X.; Cameron, S.; Costello, C.; Kirz, J.; Williams, S. *Science* **1992**, *258*, 972.
(38) Stöhr, J. *NEXAFS Spectroscopy*; Springer-Verlag: Berlin, 1992; Vol. 25.
(39) Ade, H. *Trends Polym. Sci.* **1997**, *5*, 58.
(40) Kikuma, J.; Tonner, B. P. *J. Electron. Spectrosc. Relat. Phenom.* **1996**, *82*, 53.
(41) Smith, A. P.; Spontak, R. J.; Koch, C. C.; Smith, S. D.; Ade, H. *Macromol. Mater. Eng.* **2000**, *274*, 1.
(42) Bucknall, C. B.; Partridge, I. K.; Ward, M. V. *J. Mater. Sci.* **1984**, *19*, 2064.
(43) Wrotecki, C.; Heim, P.; Gaillard, P. *Polym. Eng. Sci.* **1991**, *31*, 218.
(44) Gloaguen, J. M.; Steer, P.; Gaillard, P.; Wrotecki, C.; Lefebvre, J. M. *Polym. Eng. Sci.* **1993**, *33*, 748.

MA991453V